

# Use of a Ferritin L134P Mutant for the Facile Conjugation of Prussian Blue in the Apoferritin Cavity

Yuta Ikenoue, Yuhei O. Tahara, Makoto Miyata, Takanori Nishioka, Shigetoshi Aono, Hiroshi Nakajima

<b>Citation</b>	Inorganic Chemistry. 60(7); 4693-4704.
<b>Issue Date</b>	2021-03-18
<b>Type</b>	Journal Article
<b>Textversion</b>	Author
<b>Supporting Information</b>	The Supporting Information is available free of charge at <a href="https://pubs.acs.org/doi/10.1021/acs.inorgchem.0c03660">https://pubs.acs.org/doi/10.1021/acs.inorgchem.0c03660</a> .
<b>Rights</b>	This document is the Accepted Manuscript version of a Published Work that appeared in final form in Inorganic Chemistry, copyright © American Chemical Society after peer review and technical editing by the publisher. To access the final edited and published work see <a href="https://doi.org/10.1021/acs.inorgchem.0c03660">https://doi.org/10.1021/acs.inorgchem.0c03660</a>
<b>DOI</b>	10.1021/acs.inorgchem.0c03660

Self-Archiving by Author(s)  
Placed on: Osaka City University Repository

Ikenoue, Y., Tahara, Y. O., Miyata, M., Nishioka, T., Aono, S., & Nakajima, H. (2021). Use of a Ferritin L134P Mutant for the Facile Conjugation of Prussian Blue in the Apoferritin Cavity. *Inorganic Chemistry*, 60(7), 4693–4704. <https://doi.org/10.1021/acs.inorgchem.0c03660>

# Use of a ferritin L134P mutant for the facile conjugation of Prussian blue in the apoferritin cavity

*Yuta Ikenoue,<sup>†</sup> Yuhei O. Tahara,<sup>‡, #</sup> Makoto Miyata,<sup>‡, #</sup> Takanori Nishioka,<sup>†</sup> Shigetoshi Aono,<sup>§, □</sup> and Hiroshi Nakajima<sup>\*, †</sup>*

<sup>†</sup>Division of Molecular Materials Science, Graduate School of Science, Osaka City University, 3-3-138 Sugimoto, Sumiyoshi-ku, Osaka 558–8585, Japan.

<sup>‡</sup>Division of Biology & Geosciences, Graduate School of Science, Osaka City University, 3-3-138 Sugimoto, Sumiyoshi-ku, Osaka 558–8585, Japan.

<sup>#</sup>The OCU Advanced Research Institute for Natural Science and Technology (OCARINA), Osaka City University, Osaka 558–8585, Japan.

<sup>§</sup>Department of Creative Research, Exploratory Research Center on Life and Living Systems (ExCELLS), National Institutes of Natural Sciences, 5-1 Higashiyama, Myodaiji-cho, Okazaki 444-8787, Japan.

<sup>□</sup>Institute for Molecular Science, National Institutes of Natural Sciences, 5-1 Higashiyama, Myodaiji-cho, Okazaki 444-8787, Japan.

## KEYWORDS

Ferritin, L134P mutant, Prussian blue, Clathrate, Metal ion exchange, Oxidoreductive catalyst

## ABSTRACT

Since the bullfrog H-ferritin L134P mutant in which leucine 134 is replaced with proline was found to exhibit a flexible conformation in the  $C_3$  axis channel, homologous ferritins with the corresponding mutation have often been studied in terms of a mechanism of iron release from the mineral core within the protein cavity. Meanwhile, a ferritin mutant with the flexible channel is an attractive material in developing a method to encapsulate functional molecules larger than mononuclear ions into the protein cavity. This study describes the clathrate with a horse spleen L-ferritin L134P mutant containing Prussian blue (PB) without a frequently used technique, disassembly and reassembly of the protein subunits. The spherical shell of ferritin was confirmed in a TEM image of the clathrate. The produced clathrate (PB@L134P) was soluble in water and reproduced the spectroscopic and electrochemical properties of PB prepared using the conventional method. The catalytic activity for an oxidoreductive reaction with  $H_2O_2$ , one of the major applications of conventional PB, was also observed for the clathrate. The instability of PB in alkaline solutions, limiting its wide applications in aqueous media, was significantly improved in PB@L134P, showing the protective effect of the protein shell. The method developed here shows that horse spleen L-ferritin L134P is a useful scaffold to produce clathrates of three-dimensional complexes with ferritin.

## INTRODUCTION

Ferritin is the ubiquitous Fe storage protein that ensures a constant cellular iron level.<sup>1, 2</sup> This protein consists of 24 subunits that form a hollow dodecahedron assembled with octahedral (432) symmetry. The protein shell is penetrated by two types of channels along six  $C_4$  and eight  $C_3$  symmetry axes. The  $C_3$  axis channel serves as the pathway for iron uptake into the cavity.<sup>3-5</sup> Cytoplasmic  $\text{Fe}^{\text{II}}$  ions penetrate the protein shell through the channel and migrate to the ferroxidase center in the middle of the H-subunit under the guidance of the negatively charged side chains arranged on the interior surface of the protein shell. The  $\text{Fe}^{\text{II}}$  ions are oxidized at the ferroxidase center to  $\text{Fe}^{\text{III}}$  and then sent to the mineral growth site to be converted to a ferrioxide mineral nucleus. According to studies by Theil *et al.*,<sup>6-8</sup> replacement of leucine 134 (Leu134) in the H-subunit of bullfrog ferritin disrupts the hydrogen bonding network and some hydrophobic interactions in a subunit, resulting in the local disorder of the secondary structure forming the  $C_3$  axis channel, with no significant effect on the spherical conformation. In the crystal structure of the M-ferritin L134P mutant (PDB: 1BG7), in which Leu134 is replaced with proline, the iron uptake channel appears to be in the open conformation due to the structural disorder in the ends of the C and D helices of the subunits.<sup>6</sup> Indeed, the  $\text{Fe}^{\text{II}}$  ion that is reductively released from the ferrioxide mineral core is more reactive toward an iron chelator, such as 2,2'-bipyridine, in the L134P mutant than in the wild type protein.<sup>6, 7</sup> This difference is ascribed to the more facile penetration of the iron chelator into the cavity of the mutant, supporting the open conformation of the iron uptake channel, even in solution. A similar result is also obtained with the human H-ferritin L138P mutant that corresponds to the L134P mutant of bullfrog H-ferritin, inferring the common function of the conserved leucine residue in the conformational regulation of the  $C_3$  axis channel.<sup>9</sup> These findings have been often discussed in terms of a mechanism of iron release from

the mineral core through the uptake channel,<sup>6-10</sup> while the open channel is attractive from the perspective of developing a method to encapsulate molecules larger than mononuclear ions into the ferritin cavity.

Currently, two types of major methods have been developed to incorporate molecules into the cavity of the wild type protein.<sup>11, 12</sup> Mixing at relatively high temperatures (~60 °C) has been applied to some catalyst precursors of metal complexes.<sup>13</sup> The complexes dissociatively diffuse into the cavity and are fixed on the interior surface through coordination by amino acid residues. The coordination prevents the incorporated complex from leaking outwards. Another method consists of disassembling the cage structure of ferritin under acidic or alkaline conditions (pH < 2 or >10) into subunits, followed by reassembling the original conformation at neutral pH in the presence of the substrate molecules to be encapsulated.<sup>14-17</sup> Depending on the stoichiometric ratio of the substrate to the protein, the substrate should be enclosed in the reassembled cavity. However, this method often results in the unexpected coprecipitation of the protein with the substrate in the reaction mixture.<sup>15</sup> Dissociation of the ferritin cage with denaturing agents such as urea has also been applied instead of reducing the pH of the reaction mixture.<sup>18</sup> This method is advantageous for encapsulating substrate molecules at neutral pH, while the coprecipitation problem of the protein with the substrate has not been resolved using this method. Thus, the disassembly and reassembly of the protein should be avoided in the encapsulation processes to improve molecular uptake efficiency into the ferritin cavity. Attempts to apply passive diffusion to the wild type protein cavity have been reported for some metal complexes and precursors,<sup>13, 19, 20</sup> while ferritin was unstable during the uptake process, resulting in loss of most incubated proteins or low loading efficiency of the substrates. In order to address the problems, engineered ferritin with widened pores to allow substrates to penetrate the protein cavity has been produced by reconstitution from

a mixture of wild type and C-terminal truncated human H-ferritins.<sup>21</sup> The fabricated ferritin formed partially opened  $C_4$  axis channels that effectively load  $Fe^{II}$ -coordinated substrates into the cavity while maintaining the spherical shape of the protein. This study demonstrated that widened channels could be a versatile pathway to efficiently load and accumulate large molecular species into the ferritin cavity.

In the present study, we describe a method for encapsulating Prussian blue (PB) in the cavity of the recombinant homopolymeric horse L-ferritin L134P mutant (HL L134P) at ambient temperature without the disassembly and reassembly of the protein. Unlike H-subunits, L-subunits lack a specific ferroxidase center for biomineralization, although a glutamate cluster located at the middle of the B helix allows biomineralizing iron ions slowly.<sup>22-25</sup> Therefore, HL L134P is suitable for the present study since this mutant is expected to lack the ferroxidase center that could hamper PB production by intercepting iron ions and producing the ferrioxide mineral core. PB is a polymeric cyano-bridged metal complex with a reticular structure.<sup>26, 27</sup> Numerous studies have examined the electrochromic,<sup>28, 29</sup> photophysical,<sup>30-32</sup> magnetic,<sup>33, 34</sup> and catalytic activities of PB and its derivatives.<sup>35-37</sup> Encapsulation of PB in a water-soluble capsule is expected to overcome the inherent insolubility of PB and extend the potential use of this material, particularly in aqueous media. Although PB has been encapsulated in the cavity of the wild type protein using the disassembly and reassembly technique,<sup>38</sup> use of HL L134P provides an alternative route for incorporating ferricyanide species ( $[Fe(CN)_6]^{3-}$ ) into the intact form of the mutant and efficiently obtains the clathrate of PB (PB@L134P). PB@L134P reproduced the spectroscopic properties and electrochemistry of PB prepared using the conventional method while displayed improved resistance to alkaline solutions compared to the conventional one. PB@L134P showed high catalytic activity in the oxidoreductive reaction using  $H_2O_2$  as an oxidant. Some mechanistic

analyses for the reaction inferred another catalytic cycle different from that reported for conventional PB.<sup>37</sup> The pH-dependent shift of the IVCT band and the reaction with potassium cyanide indicated that PB in the clathrate was enriched at the vacant coordination sites on the iron ions, which were associated with the high catalytic activity of PB@L134P.

## RESULTS AND DISCUSSION

**Synthesis of PB@L134P.** Although the flexible loop conformation at the ends of C and D helices, which is observed for bullfrog H-ferritin L134P and human H-ferritin L138P mutants, has not been reported in HL L134P, we expected that the replacement of conserved Leu134 with proline affected the same conformational effect on the horse spleen L-ferritin: the overall sequence identities and similarity of horse spleen L-ferritin with bullfrog H-ferritins are 58.5 and 88.6%, respectively, which are comparable to those of human H-ferritin with bullfrog H-ferritin (65.6 and 90.7%, respectively) (Figure S1). HL L134P was overproduced in *E. coli* and purified using a previously reported method.<sup>13</sup> SDS-PAGE showed no apparent contaminating proteins in the purified sample (Figure S2a). The TEM image of the purified protein negatively stained with 2% ammonium molybdate showed spherical shells with an outer diameter of ca.12 nm, confirming that the HL L134P maintained the characteristic conformation of ferritin (Figure S2b). Some cavities were stained with ammonium molybdate penetrated, while no ferrioxide core, which formed black spots inside the shell,<sup>39</sup> was observed. The UV-Vis spectrum of HL L134P showed a unique absorption band at 278 nm derived from tyrosine and tryptophan residues, with a molar extinction coefficient of  $4.6 \times 10^5 \text{ M}^{-1}\text{cm}^{-1}$  (Figure S2c). Consistent with the results of the TEM images, no trace of the ferrioxide core, which shows a wide, featureless band over the entire visible region, was observed in the spectrum.<sup>25</sup> The circular dichroism (CD) spectrum of HL L134P showed peaks of a negative Cotton effect at 210 and 222 nm, which are characteristic of  $\alpha$ -helices with the molar

ellipticity value of  $-2.0 \times 10^4$  deg cm<sup>2</sup>dmol<sup>-1</sup> at 222 nm (Figure S2d). This is 20% smaller than that of the recombinant horse L-ferritin wild type (HL WT,  $-2.5 \times 10^4$  deg cm<sup>2</sup>dmol<sup>-1</sup>) and coincident with data obtained with bullfrog H-ferritin L134P mutant (Figure S1b).<sup>7</sup> Human H-ferritin L138P shows an 8% decrease in the helix content than the wild-type protein, in approximate agreement with that of the unfolded conformation of the  $C_3$  axis channel.<sup>9</sup> Thus, the CD data supports the flexible or unfolded conformation of the  $C_3$  axis channels in HL L134P that maintains the original hollow structure of ferritin.

Mixing the purified HL L134P (5  $\mu$ M) with 1,000-fold molar equivalents of potassium ferricyanide ( $K_3[Fe(CN)_6]$ ) or potassium ferrocyanide ( $K_4[Fe(CN)_6]$ ) in 20 mM HEPES-NaOH (HEPES) buffer at pH 7.0 failed in the uptake of the complex within the protein cavity. A higher concentration of the complexes in the reaction mixture did not restore the uptake efficiency because of the substantial precipitation of the protein. Many studies on the uptake mechanism of iron ions through the  $C_3$  axis channel have pointed out the crucial role of carboxyl side chains placed in the channel.<sup>40-42</sup> The negatively charged carboxyl groups at neutral pH form the electrostatic gradient increasing across the channel inward, which is favorable to drive the positively charged iron ions into the cavity. Conversely, anionic molecules may be prevented from approaching the channel due to the electrostatic repulsion. Since horse spleen L-ferritin conserves the corresponding carboxyl side chains in Asp127 and Glu130, the result implied that the electrostatic repulsion was still effective in the channel of HL L134P on the reaction with  $[Fe(CN)_6]^{3-/4-}$  species. Thus, we decided to combine some methods to attenuate the charge repulsion and achieve the incorporation of either  $[Fe(CN)_6]^{3-}$  or  $[Fe(CN)_6]^{4-}$  species within the cavity of HL L134P.<sup>18, 43</sup> The initial step was to treat HL L134P (2  $\mu$ M) with 1,000-fold molar equivalents of copper acetate in 1 M sodium acetate (NaOAc) buffer at pH 4.2, followed by



desalting column operation and dialysis to remove the unreacted free  $\text{Cu}^{\text{II}}$  ion. In this and following steps, the pH of the reaction mixture was adjusted to 4.2, which was slightly lower than the isoelectric point of HL WT ( $\text{pI} = 4.4$ ),<sup>44</sup> to reverse the negative charge of the protein surface and cancel a possible electrostatic gradient formed by Asp127 and Glu130 in the original  $C_3$  axis channel.<sup>40-42</sup> The amount of  $\text{Cu}^{\text{II}}$  ions in the resulting protein sample was estimated to be 180 per protein, based on the results of the ICP-AES measurement and Bradford protein assay. A similar uptake ratio of divalent metal ions was reported for HL wild type,<sup>18, 45, 46</sup> indicating that HL L134P retains the capacity to accumulate metal ions at a level comparable to the wild type protein. Acetate salt was the essential source of the  $\text{Cu}^{\text{II}}$  ions. The substantial precipitation of the protein immediately followed the addition of other  $\text{Cu}^{\text{II}}$  sources such as nitrate and sulfate salts to HL L134P. A high concentration of the buffer (1 M NaOAc) was needed to enhance the effect of the acetate anion on the reaction. In the second step, HL L134P containing  $\text{Cu}^{\text{II}}$  ions was mixed with 1,000-fold molar equivalents of  $\text{K}_3[\text{Fe}(\text{CN})_6]$  in 20 mM NaOAc buffer at pH 4.2, anticipating that the  $\text{Cu}^{\text{II}}$  ions fixed on the interior surface of the protein would tether the penetrated  $[\text{Fe}(\text{CN})_6]^{3-}$  species through the formation of  $\text{Fe}^{\text{III}}\text{-CN-Cu}^{\text{II}}$  bonds. The reaction mixture gradually formed a yellowish precipitate, which was collected by centrifugation and washed several times with HEPES buffer to remove the residual  $[\text{Fe}(\text{CN})_6]^{3-}$  species. The precipitate was dissolved in HEPES buffer by prolonged sonication. Gel permeation chromatography with the dissolved precipitate provided a single major fraction, which showed a band at the migration distance almost the same as the intact HL L134P in Native PAGE (Figure S3a and b). TEM image of the same sample found the spherical shells similar to the intact mutant (Figure S3c). These results indicated that HL L134P in the precipitate maintained the original conformation. The IR spectra of the precipitate before and after dissolved in the buffer were shown in Figures 1a and b, respectively. Both spectra show

bands at 1650, 1540, and 2109  $\text{cm}^{-1}$ , which correspond to the amide I, II bands from the main chain of HL L134P and  $\nu(\text{C-N})$  of  $[\text{Fe}(\text{CN})_6]^{3-}$ , respectively.

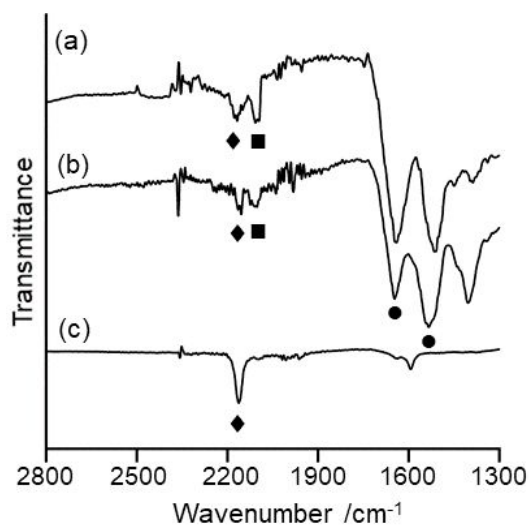


**Figure 1.** IR spectra of the precipitate obtained in the second step of PB clathrate production (a) before and (b) after dissolution to HEPES buffer. (c) the copper substituted PB derivative, where the  $\text{Fe}^{\text{II}}$  ions were replaced with  $\text{Cu}^{\text{II}}$  ions.<sup>47</sup> Labels on the spectra: (●), amide I (1650  $\text{cm}^{-1}$ ) and II (1540); (■),  $\nu(\text{C-N})$  of  $[\text{Fe}(\text{CN})_6]^{3-}$  (2109); (♦),  $\nu(\text{C-N})$  of the  $\text{Fe}^{\text{III}}\text{-CN-Cu}^{\text{II}}$  unit (2162).

A band at 2162  $\text{cm}^{-1}$  coincides with  $\nu(\text{C-N})$  of a  $\text{Fe}^{\text{III}}\text{-CN-Cu}^{\text{II}}$  unit in a copper-substituted PB derivative<sup>47</sup> (Figure 1b), suggesting the formation of a bond between the interior  $\text{Cu}^{\text{II}}$  ions with the penetrated  $[\text{Fe}(\text{CN})_6]^{3-}$  species. The use of the same procedure with HL WT in place of HL L134P resulted in the recovery of the protein incorporating only  $\text{Cu}^{\text{II}}$  ions. IR absorption bands characteristic of  $\nu(\text{C-N})$  were not observed for the recovered protein. Domínguez-Vera *et al.* reported consistent data with the current result.<sup>18</sup> They treated HL WT with urea to relax the structure of the iron uptake channel. The treatment allowed  $[\text{Fe}(\text{CN})_6]^{3-}$  to penetrate the cavity of HL WT; otherwise, HL WT incorporating  $\text{Cu}^{\text{II}}$  ions failed to react with  $[\text{Fe}(\text{CN})_6]^{3-}$ . Based on these results, a reasonable conclusion would be that the  $[\text{Fe}(\text{CN})_6]^{3-}$  species were not trapped on the

exterior surface of HL L134P but penetrated the cavity through the open channel. The  $\text{Cu}^{\text{II}}$  ions within the cavity formed  $\text{Fe}^{\text{III}}\text{-CN-Cu}^{\text{II}}$  bonds and were likely to restrain the rediffusion of  $[\text{Fe}(\text{CN})_6]^{3-}$  species from the cavity to the bulk solution. The final step in the production of PB@L134P was replacing the  $\text{Cu}^{\text{II}}$  ions within the HL L134P cavity with  $\text{Fe}^{\text{II}}$ , which was achieved by mixing the precipitate obtained in the previous step with 100 mM  $\text{FeSO}_4$  in HEPES buffer under anaerobic conditions. The metal ion exchange reaction in PB analogs was reported to be a versatile method for designing and preparing PB-based solid catalysts.<sup>43</sup> After incubation for a day, the yellowish precipitate in the  $\text{FeSO}_4$  solution turned bluish. The bluish precipitate was repeatedly washed with HEPES buffer until the effluent became unresponsive to the colorimetric detection of free iron ions. The washed product was not readily soluble, while extensive sonication effectively dissolved the product in HEPES buffer. Once dissolved, no precipitation appeared, even after centrifugation at 22,000 g for 30 min at 4 °C (Figure S4).

The IR spectra recorded before and after dissolving the final product in the buffer were virtually identical (Figure 2).

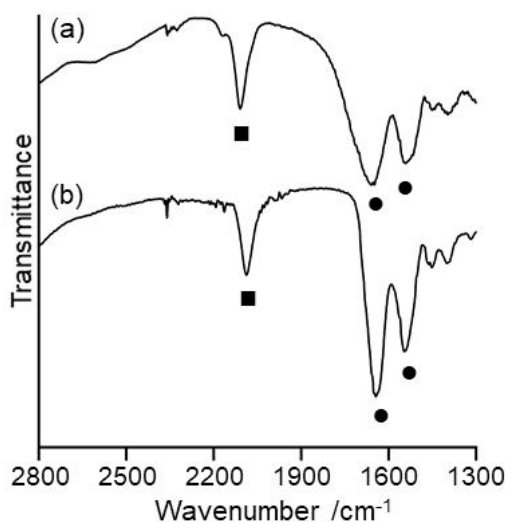


**Figure 2.** The IR spectra recorded (a) before and (b) after dissolving the final product in HEPES buffer. The product dissolved in the buffer solution was desalted by column operation and dried

by blowing with air on an ATR unit installed in a spectrometer before measurement. Labels on the spectra: (●), amide I ( $1650\text{ cm}^{-1}$ ) and II ( $1540$ ); (■),  $\nu(\text{C-N})$  of  $[\text{Fe}(\text{CN})_6]^{3-}$  ( $2109$ ).

The  $\nu(\text{C-N})$  of the  $\text{Fe}^{\text{III}}\text{-CN-Cu}^{\text{II}}$  bond observed for the yellowish precipitate ( $2162\text{ cm}^{-1}$ ) is replaced with a new band at  $2084\text{ cm}^{-1}$ , which coincides with  $\nu(\text{C-N})$  of a  $\text{Fe}^{\text{II}}\text{-CN-Fe}^{\text{III}}$  unit in PB.<sup>38</sup> The band associated with free  $[\text{Fe}(\text{CN})_6]^{3-}$  ( $2109\text{ cm}^{-1}$ ) has disappeared, while the amide I and II bands ( $1650$  and  $1540\text{ cm}^{-1}$ , respectively) from the protein main-chain remains. In the UV-Vis spectrum, the dissolved product shows shoulder and broad bands at  $278$  and  $700\text{ nm}$ , respectively, the latter of which is characteristic of the intervalence charge transfer band (IVCT) observed for the  $\text{Fe}^{\text{II}}\text{-CN-Fe}^{\text{III}}$  units in PB (Figure 3).<sup>32</sup> The TEM image of the dissolved product shows monodispersed spherical shells with an outer diameter of ca.  $12\text{ nm}$  (Figure 4), consistent with the molecular shape of the intact HL L134P (Figure S2b).

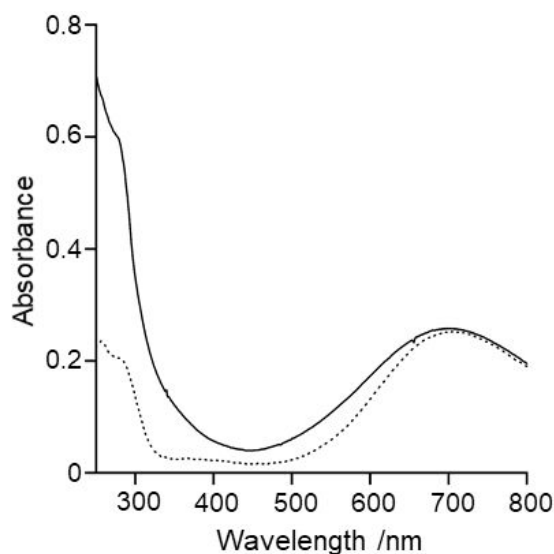


**Figure 3.** UV-Vis spectra of the bluish product dissolved in HEPES buffer (—). The protein concentration was adjusted to  $0.3\text{ }\mu\text{M}$  in the solution sample based on the Bradford protein assay.

The spectrum of conventionally prepared colloidal PB is also shown for comparison (---). The absorbance of both spectra is adjusted at the maximum of the IVCT band.

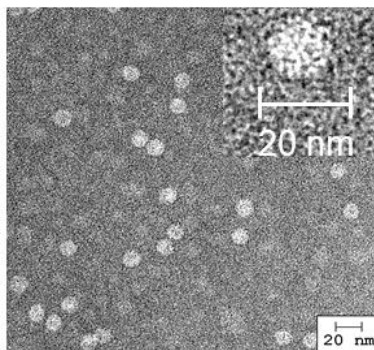


**Figure 4.** TEM image of the bluish product (24 mg protein/L) dissolved in HEPES buffer. The sample was negatively stained with 2 % ammonium molybdate.

Non-productive coprecipitation of the protein with the metal ion or metal complex was not observed throughout the processes. The molar ratio of PB in PB@L134P was approximately estimated to be 36 in terms of  $\text{Fe}_4[\text{Fe}(\text{CN})_6]_3$  by applying the molar extinction coefficients ( $2.4 \times 10^4 \text{ M}^{-1} \text{ cm}^{-1}$  at 700 nm, See SI) calculated from that of PB nanoparticles reported previously<sup>32</sup> and the result of Bradford protein assay with PB@L134P. ICP-AES measurement to accurately quantify the iron ions resulted in the apparent overestimation of iron, which was probably attributed to the residual iron ions tightly bound interior surface of HL L134P. The residual iron ions were confirmed in the UV-Vis spectrum of PB@L134P as a featureless shoulder band at 350 nm, which was observed for HL L134P incorporating  $\text{Fe}^{\text{III}}$  ions (Figure S5). Less than 20 copper ions were detected in PB@L134P by ICP-AES measurement, indicating the replacement with the  $\text{Fe}^{\text{II}}$  ions added at the final process for producing PB@L134P. One may propose an immediate reaction of  $[\text{Fe}(\text{CN})_6]^{4-}$  or  $[\text{Fe}(\text{CN})_6]^{3-}$  with HL L134P incorporating  $\text{Fe}^{\text{III}}$  or  $\text{Fe}^{\text{II}}$  ions in place of  $\text{Cu}^{\text{II}}$ . However, the  $\text{Fe}^{\text{III}}$  ions preloaded to HL L134P did not react with  $[\text{Fe}(\text{CN})_6]^{3-}$  and  $[\text{Fe}(\text{CN})_6]^{4-}$ .

, resulting in the recovery of the original reactants. The different behavior between the  $\text{Cu}^{\text{II}}$  and  $\text{Fe}^{\text{III}}$  ions can be accounted for by the formation of the iron cluster ( $\mu^3$ -oxo)tris[( $\mu^2$ -peroxo)]tri-iron(III) species in the interior surface of L-ferritin.<sup>25, 48</sup> The stable iron cluster probably prevents the reaction of  $\text{Fe}^{\text{III}}$  ions with  $[\text{Fe}(\text{CN})_6]^{3-}$  and  $[\text{Fe}(\text{CN})_6]^{4-}$ . The  $\text{Fe}^{\text{II}}$  ion was readily oxidized to  $\text{Fe}^{\text{III}}$  within the cavity unless anaerobic conditions were maintained in all processes before reacting with  $[\text{Fe}(\text{CN})_6]^{3-}$ . The cumbersome anaerobic conditions impaired the reproducibility of the molecular properties and synthetic yield of PB@L134P. Because of the facile replacement with iron ions in a metal substituted PB analogues<sup>43</sup> and inertness to oxidation under aerobic conditions,  $\text{Cu}^{\text{II}}$  was the appropriate ion initially introduced to HL L134P.

The protein shell of PB@L134P was digestible with proteinase K (Figure 5a). The complete digestion and subsequent purification by gel permeation chromatography provided a water-soluble blue species (PB@L134P/p), which showed the absorption bands of amide I and II as well as  $\nu(\text{C}-\text{N})$  of the  $\text{Fe}^{\text{II}}-\text{CN}-\text{Fe}^{\text{III}}$  unit in the IR spectrum (Figure 5b).

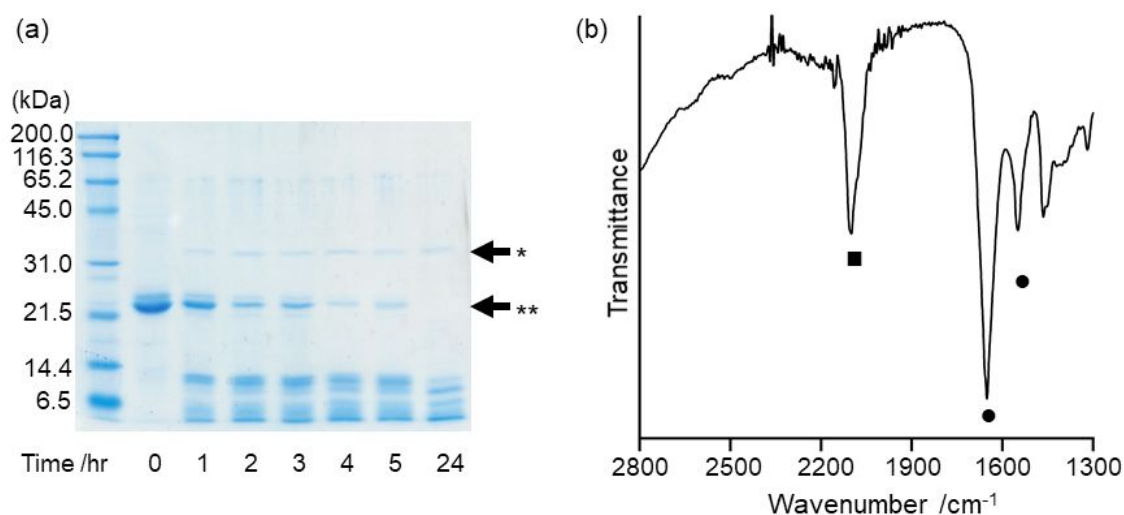


**Figure 5.** Digestion of PB@L134P with Proteinase K (a) Complete digestion of the protein shell was achieved in 24hrs under current reaction conditions. The digestion process was monitored by

SDS-PAGE. \*proteinase K; \*\*PB@L134P. (b) A water-soluble blue species purified from the digested PB@L134P (PB@L134P/p) shows bands of amide I, II (●, 1650 and 1549  $\text{cm}^{-1}$ , respectively) and  $\nu(\text{C-N})$  of the  $\text{Fe}^{\text{II}}\text{-CN-Fe}^{\text{III}}$  unit (■, 2098  $\text{cm}^{-1}$ ) in the IR spectrum.

The MALDI-TOF mass spectrum of PB@L134P/p showed three dominant signals at  $m/z = 2499.88$ , 4971.94, and 5563.20, confirming protein fragment(s) in PB@L134P/p (Figure 6a).

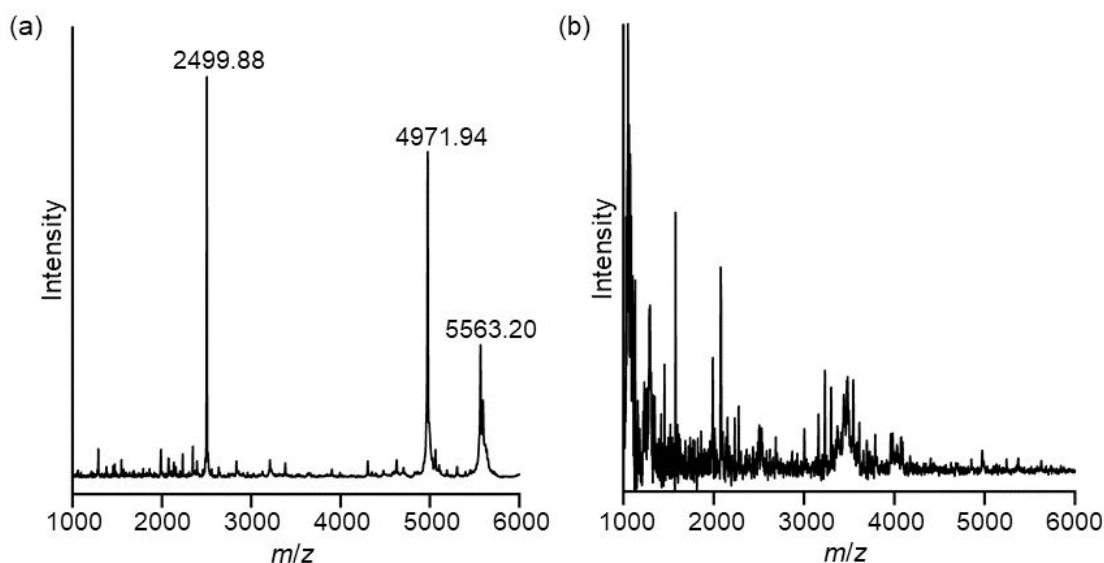


**Figure 6.** MALDI-TOF mass spectra. (a) PB@L134P/p showed three major signals. (b) the intact HL L134P after the same protease K treatment as PB@L134P.

A plausible interpretation of the results is that in PB@L134P, there was an interaction between the PB species with the protein shell, which was retained in a composite with a protein fragment even after the protein digestion. The corresponding mass signals were not observed for the intact HL L134P after the same protease treatment as PB@L134P, indicating that the PB species in PB@L134P/p was protective of the interacting fragment from further digestion by protease K (Figure 6b).

Table 1 shows putative protein fragments with monoisotopic masses consistent with the observed signals within  $\Delta m/z = 1$ , which was determined from the mass accuracy of the instrument used in the current study. Among them, the fragments included in the A, C helices or loop (R25-E45 and Q69-W89) are unlikely to be candidates for the observed signals since they are arranged in the exterior surface of the protein shell (Figure S6).

**Table 1.** Protein fragments with monoisotopic masses assignable to the observed mass signals in PB@L134P/p.

Observed	2499.88	4971.94	5563.20
Protein fragments* (Monoisotopic mass $[M+H]^+$ )	Arg25-Glu45 (2500.19)	Gly34-Arg75 (4971.44)	Leu113-Glu163 (5563.80)
	Gln69-Trp89 (2500.22)	Asp127-Leu169 (4971.56)	
	Lys143-Leu165 (2499.29)		

\*The initial methionine residue is removed from the primary sequence. The sequence number is started at the second residue, serine.

The L113-E163 was the unique fragment that matched the observed signal at  $m/z = 5563.20$  and overlapped with the D127-L169 fragment in the C-terminal region of the D helix. The K143-L165 fragment also shared a similar region with the L113-E163 and D127-L169 fragments. From the above considerations, it is possible that some of the D-helix was involved in the interaction of the protein shell with the internal PB.

**Stability of PB@L134P in alkaline solutions.** PB is unstable in alkaline solutions due to solubilization by hydroxy ions,<sup>49</sup> although the detailed solubilization mechanism remains to be solved. The cavity of HL L134P is connected to the external environment through the wide-open



iron uptake channel, while the protein shell may restrict the contact of PB with the bulk solution. Consequently, the solubilization of PB in PB@L134P would be prevented to some degree. Based on this hypothesis, the solubilization kinetics of PB in alkaline solutions were studied for PB@L134P in comparison with colloidal PB prepared conventionally. Representative changes in UV-Vis spectra of PB@L134P and colloidal PB upon introduction to the 20mM HEPES buffer at pH 8.0 are shown in Figure 7.

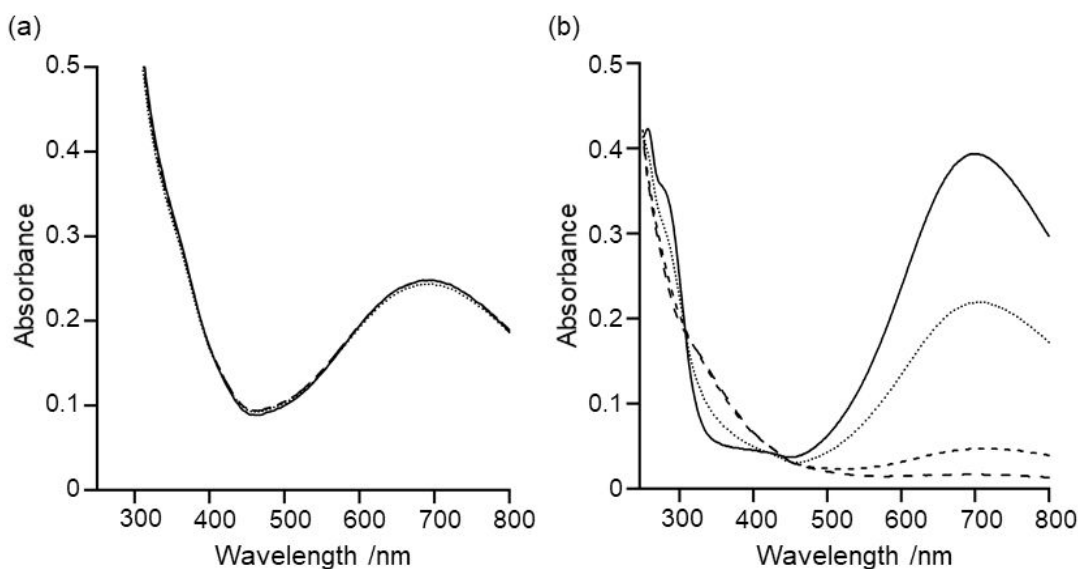


**Figure 7.** UV-Vis spectral changes of (a) PB@L134P and (b) colloidal PB after dissolution in the 20 mM HEPES buffer at pH 8.0. In (a), the spectra were recorded at 0 (—), 30 (----), 60 (- -), and 90 (- -) min after the dissolution. In (b), the spectra were recorded at 0 (—), 10 (-----), 20 (- -), and 30 (- -) min after the dissolution.

Compared to colloidal PB, a significantly slower decrease in the IVCT bands was observed for PB@L134P. PB@L134P retained its blueish color for more than half a month at ambient temperature, while the color of colloidal PB was almost extinguished in an hour. The time courses

of the PB solubilization at pH 8 - 10 traced by the disappearance of the IVCT band are shown in Figures 8a and b.

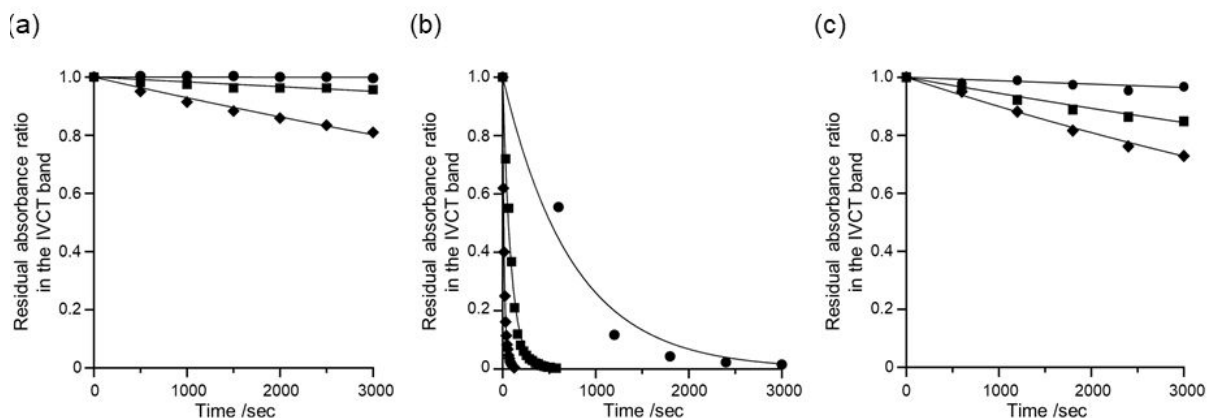


**Figure 8.** Plots of solubilization kinetics for (a) PB@L134P, (b) colloidal PB, and (c) PB@L134P/p recorded at pH 8.0 (●), pH 9.0 (■), and pH 10.0 (◆). Regression curves for each dataset were produced from first-order kinetic equations with parameters described in Table 2.

The solubilization kinetics was not examined in solutions at a pH greater than 10 due to the disassembly of the protein.<sup>50</sup> The obtained decay plots were apparently reproduced with the first-order kinetic equations, while no plausible model has been obtained for the kinetic data. The rate constants of PB@L134P and colloidal PB in different pH solutions at ambient temperature are listed in Table 2. Although the stability of the PB@L134P was reduced at higher pH, the rate constants of PB@L134P were significantly smaller than colloidal PB at each pH value examined, showing the superior stability of PB@L134P to colloidal PB in alkaline solutions. Despite removing the protein shell, PB@L134P/p maintained a higher resistance to alkaline conditions than colloidal PB (Figure 8c and Table 2). This suggests that in addition to decoupling the inner cavity of PB@L134P from the bulk solution, the protein shell has another mechanism to protect the interior PB through the direct interaction and improve the stability of PB@L134P in alkaline solutions.

**Table 2.** Rate constants of the solubilization reaction ( $\text{s}^{-1}$ ) at ambient temperature for PB@L134P, PB@L134P/p, and colloidal PB in alkaline solutions.

	pH		
	8.0	9.0	10.0
PB@L134P	$3.4 \times 10^{-7}$	$1.7 \times 10^{-5}$	$7.4 \times 10^{-5}$
PB@L134P/p	$1.3 \times 10^{-5}$	$6.1 \times 10^{-5}$	$1.1 \times 10^{-4}$
Colloidal PB	$1.4 \times 10^{-3}$	$1.1 \times 10^{-2}$	$5.6 \times 10^{-2}$

Another feature of PB@L134P in alkaline solution was the blueshift of the IVCT band. The absorption maximum of 700 nm at pH 7.0 shifted to 686 nm at pH 8.0, while the absorption maximum of colloidal PB was insensitive to the solution pH. The more prominent blueshift was observed when PB@L134P was dissolved in the buffer solution pH 9.0 ( $\lambda_{\text{max}} = 590\text{nm}$ ) (Figure S7a). This shift was virtually reversible. The IVCT band was pulled back to the original wavelength by adjusting the solution pH to 7.0 except for some decrease in the absorbance. The IVCT band of colloidal PB was observed at an almost identical wavelength at pH 7.0 (700 nm) and 9.0 (690 nm), although the absorbance of the band rapidly diminished at the higher pH as expected from the instability of colloidal PB in alkaline solution (Figure S7b). Thus, the observed IVCT band shift of PB@L134P was not involved in the solubilization processes of PB. The surface of PB particles contains some vacant coordination sites on  $\text{Fe}^{\text{III}}$  ions occupied by water molecules.<sup>26</sup> The vacant sites do not affect the properties of nanosized colloidal PB, probably because of the low population compared to the total number of  $\text{Fe}^{\text{III}}$  ions in the colloidal PB. Conversely, PB with smaller dimensions in PB@L134P could be more susceptible to ligands coordinated to the vacant sites. As described above, the molar ratio of  $\text{Fe}_4[\text{Fe}(\text{CN})_6]_3$  to the protein in PB@L134P was estimated to be 36. A possible interpretation of this number is a cuboidal PB

composed of 6-7 iron ions on a side. Alternatively, assuming that there are PB species homogeneously distributed in the D helix of each subunit, the number of iron ions in the single PB species is approximately 10, which corresponds to the almost smallest PB unit. PB with such small dimensions should have a higher proportion of iron ions with vacant coordination sites on the cubic surface than colloidal PB. Treatment of PB@L134P with potassium cyanide (KCN) to mask the vacant sites with external  $\text{CN}^-$  ligands provided experimental support to the susceptibility of the IVCT band to the alkaline conditions. The KCN treatment was performed by adding KCN (1 mM at the final concentration) to PB@L134P solution (adjusted to 20  $\mu\text{M}$  based on  $\text{Fe}_4[\text{Fe}(\text{CN})_6]_3$ ), followed by purification on a desalting column. Although the resulting PB@L134P showed no apparent changes in the UV-Vis spectrum except for some decrease in the absorbance at pH 7.0, the IVCT band turned insensitive to the alkaline conditions (pH 9.0) with further improved stability (Figure 9).

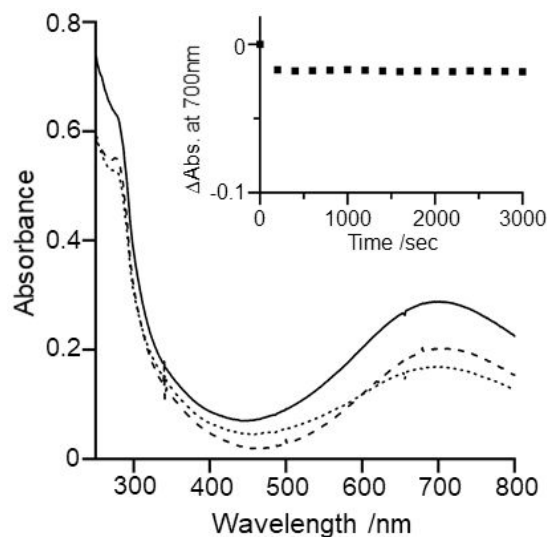


**Figure 9.** UV-Vis spectra of PB@L134P in HEPES buffer at pH 7.0 before (—) and after (---) KCN treatment. (····), the KCN treated PB@L134P in the 20 mM CHES buffer at pH 9.0. The sample concentration after the KCN treatment was adjusted with the protein concentration

determined by the Bradford method. Inset, the time course of the IVCT band's absorbance of the KCN treated PB@L134P upon dissolution in the CHES buffer at pH 9.0.

The partial decrease in absorbance and broadening to the shorter wavelength region observed in the IVCT band at pH 9.0 is a possible vestige of unreacted vacant sites with  $\text{CN}^-$ . Thus, masking the vacant sites with the external  $\text{CN}^-$  ligand inhibited the IVCT band shift and further improved the stability of PB in the alkaline solution. This result supports that the coordination of water or hydroxyl ion to the vacant sites of the interior PB depending on the solution pH invokes the shift of the IVCT band of PB@L134P, while the vacant sites are not the origin of tolerance to alkaline conditions.

**Electrochemical property of PB@L134P.** Previous studies with ferritin incorporating some redox active species or mineral cores have indicated that the protein shell is electrochemically active and transfers electrons between the electrode and interior species.<sup>51-53</sup> This behavior was also observed for PB@L134P. The cyclic voltammogram of PB@L134P shows a redox couple with the midpoint potential of 0.43 V (vs. SHE) (Figure 10) that coincides with the redox couple of  $\text{Fe}^{\text{II}}\text{-CN-Fe}^{\text{III}}/\text{Fe}^{\text{II}}\text{-CN-Fe}^{\text{II}}$ .<sup>49</sup> The redox couple of  $\text{Fe}^{\text{II/III}}$  residually bound to the interior surface of HL L134P was not assignable to the observed couple, as it was observed at 0.23 V (Figure S8). Although another redox couple corresponding to  $\text{Fe}^{\text{II}}\text{-CN-Fe}^{\text{III}}/\text{Fe}^{\text{III}}\text{-CN-Fe}^{\text{III}}$  was not observed under the present measurement conditions, the PB in PB@L134P was a redox active component through the protein shell.

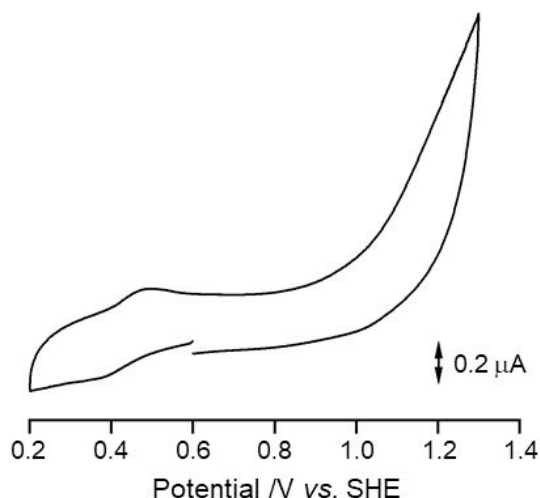


**Figure 10.** Cyclic voltammogram of PB@L134P in HEPES buffer at pH 7.0 containing 0.1 M KCl as an electrolyte. The sample concentration was adjusted to 20  $\mu\text{M}$  based on  $\text{Fe}_4[\text{Fe}(\text{CN})_6]_3$ . WE: glassy carbon ( $\phi = 3$  mm); CE: Pt wire; RE: Ag/AgCl; scan rate: 50 mV/s.

**The activity of PB@L134P as an oxidoreductive catalyst.** One of the major applications of PB is in the catalytic reduction of  $\text{H}_2\text{O}_2$ , where the  $\text{Fe}^{\text{II}}\text{-CN-Fe}^{\text{II}}$  unit electrochemically generated on a cathodic electrode is the active species that reduces  $\text{H}_2\text{O}_2$  to hydroxyl ions.<sup>49</sup> Meanwhile, according to Zhang *et al.*, the  $\text{Fe}^{\text{II}}\text{-CN-Fe}^{\text{III}}$  units of PB (oxidation potential: 0.9 V) and Berlin Green (oxidation potential: 1.4 V), the mixture of the  $\text{Fe}^{\text{II}}\text{-CN-Fe}^{\text{III}}$  and  $\text{Fe}^{\text{III}}\text{-CN-Fe}^{\text{III}}$  units, has the potential to mediate the reduction of  $\text{H}_2\text{O}_2$  because of the standard reduction potential of 1.8 V for  $\text{H}_2\text{O}_2 + 2\text{H}^+ + 2\text{e}^- \rightarrow 2\text{H}_2\text{O}$ .<sup>37</sup> The formed  $\text{Fe}^{\text{III}}\text{-CN-Fe}^{\text{III}}$  units are reverted to  $\text{Fe}^{\text{II}}\text{-CN-Fe}^{\text{III}}$  in the presence of a reducing substrate. Thus, PB serves as an oxidoreductive catalyst with  $\text{H}_2\text{O}_2$  as the oxidant. As was observed for HL WT incorporating an iron-mineral core coated with a PB layer,<sup>37, 54</sup> the oxidoreductive activity was also observed for PB@L134P using 3,5,3',5'-tetramethylbenzidine (TMB) as a reductant. One electron oxidation product of TMB is in equilibrium with a stable charge-transfer complex of the diamine and diimine species, which is detectable by a characteristic absorbance at 652 nm ( $\epsilon_{652} = 3.9 \times 10^4 \text{ M}^{-1}\text{cm}^{-1}$ ).<sup>55, 56</sup> The oxidation

product was detected in the presence of  $\text{H}_2\text{O}_2$  and PB@L134P in 200 mM NaOAc buffer at pH 3.6 (Figure 11).

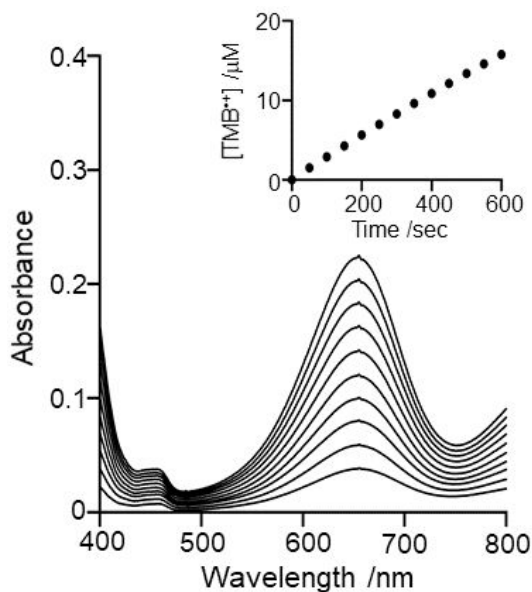


**Figure 11.** Oxidation of TMB by  $\text{H}_2\text{O}_2$  catalyzed by PB@L134P in 200 mM NaOAc buffer at pH 3.6. The UV-Vis spectrum was recorded every 1 min after starting the reaction by adding PB@L134P to the reaction mixture. The concentration of PB@L134P was adjusted to 1.0  $\mu\text{M}$  based on  $\text{Fe}_4[\text{Fe}(\text{CN})_6]_3$  estimated from the IVCT band absorbance. Inset: Time course of the oxidation product evaluated from the increase in the absorbance at 652 nm.

The lack of reaction in the absence of PB@L134P, otherwise under the same conditions, confirmed the catalytic role of PB@L134P. Meanwhile, the catalytic mechanism with PB@L134P was unlikely in the scenario proposed by Zhang *et al.* Mixing with an excess amount of  $\text{H}_2\text{O}_2$  in the same acetate buffer resulted in no changes in the UV-Vis spectrum of PB@L134P (Figure S9a). Iodometric titration showed no apparent consumption of  $\text{H}_2\text{O}_2$  in the reaction mixture without TMB (Figure S9b). The result indicated that the  $\text{Fe}^{\text{II}}\text{-CN-Fe}^{\text{III}}$  units in PB@L134P were inactive

in the reduction of  $\text{H}_2\text{O}_2$ . Instead, oxidation of TMB by PB@L134P was observed in the absence of  $\text{H}_2\text{O}_2$  (Figure 12).

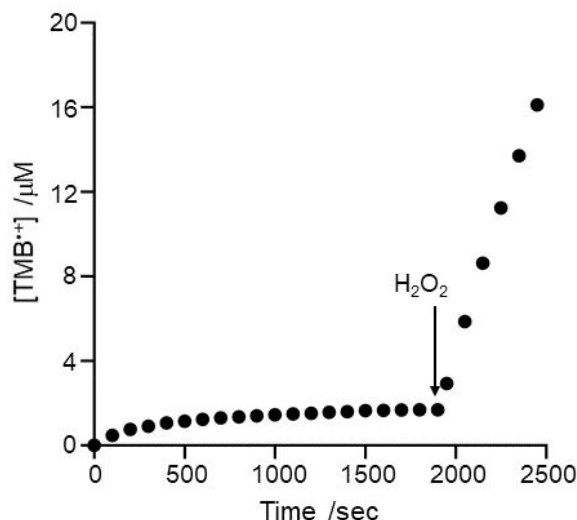


**Figure 12.** The oxidation reaction of TMB (160  $\mu\text{M}$ ) in the presence of PB@L134P (1.0  $\mu\text{M}$  based on  $\text{Fe}_4[\text{Fe}(\text{CN})_6]_3$ ). The reaction was initiated in the absence of  $\text{H}_2\text{O}_2$ . After observing no apparent increase in the oxidation product of TMB (1900 sec in the reaction period), 100  $\mu\text{M}$   $\text{H}_2\text{O}_2$  was added to the reaction mixture.

The total amount of the oxidation product in terms of the TMB cation radical was reproducibly 1.6 equivalents of  $\text{Fe}_4[\text{Fe}(\text{CN})_6]_3$  in PB@L134P. Atmospheric oxygen did not participate in the reaction, as anaerobic conditions did not affect the reaction. After the single turnover reaction, the addition of  $\text{H}_2\text{O}_2$  to the reaction mixture immediately resumed the oxidation of TMB. Thus, analogous to the electrochemical processes, the catalytic reaction of PB@L134P should start at reducing the  $\text{Fe}^{\text{II}}\text{-CN-Fe}^{\text{III}}$  units to  $\text{Fe}^{\text{II}}\text{-CN-Fe}^{\text{II}}$  with TMB, followed by the oxidation of the formed  $\text{Fe}^{\text{II}}\text{-CN-Fe}^{\text{II}}$  units to  $\text{Fe}^{\text{II}}\text{-CN-Fe}^{\text{III}}$  with  $\text{H}_2\text{O}_2$ . The residual  $\text{Fe}^{\text{III}}$  ions tightly bound to the interior surface of the protein shell (*vide supra*) could be a catalyst in the current reaction. However, this hypothesis was refused by analyzing the separately prepared HL L134P containing  $\text{Fe}^{\text{III}}$  ions,



which showed no activity in the catalytic oxidation of TMB by  $\text{H}_2\text{O}_2$ , although the current data do not exclude some assistive role of the  $\text{Fe}^{\text{III}}$  ions in the catalytic action of PB within the protein cavity.

Despite the isolated active sites from bulk solution by the protein shell, catalytic activity of PB@L134P in the TMB oxidation was more than 10-fold higher than colloidal PB when the concentration of the PB moiety was adjusted with the absorbance of the IVCT band. The turnover frequency (TOF) of PB@L134P was determined to be  $2.2 \times 10^{-2} \text{ s}^{-1}$  per  $\text{Fe}_4[\text{Fe}(\text{CN})_6]_3$  under the present experimental conditions, while that of colloidal PB was  $1.9 \times 10^{-3} \text{ s}^{-1}$ . The pH-dependent shifts of the IVCT band and the inhibitory effect of the external  $\text{CN}^-$  ligand showed that PB in PB@L134P was enriched in the vacant coordination sites on the iron ions compared to colloidal PB (*vide supra*). The vacant sites are potentially active in the catalytic reaction, resulting in the enhanced catalytic activity of PB@L134P than colloidal PB. Consistent with this assumption, PB@L134P reduced TOF for the TMB oxidation to  $5.6 \times 10^{-3} \text{ s}^{-1}$  after the KCN treatment (Figure S10). Meanwhile, the protein shell was not a crucial effector for the oxidoreductive activity of PB@L134P (Figure S10). The catalytic activity of PB@L134P was maintained by 70% ( $\text{TOF} = 1.6 \times 10^{-2} \text{ s}^{-1}$  per  $\text{Fe}_4[\text{Fe}(\text{CN})_6]_3$ ) after the protein digestion with proteinase K. Therefore, the major contributions of the protein cavity to the catalytic activity is the growth restriction of the interior PB and the consequent enrichment of the  $\text{Fe}^{\text{III}}$  ions with the vacant coordination sites.

## CONCLUSIONS

In the present study, the HL L134P mutant showed the potential to incorporate molecules with a cross-sectional area larger than the original diameter of the channel. Using the developed method, HL L134P incorporated  $[\text{Fe}(\text{CN})_6]^{3-}$  in the absence of heat treatment or any denaturation and

disassembly of the protein conformation. HL L134P provides the water-soluble cage connected to the bulk solution and limits the growth of the reticular metal complexes below the nano-scale level. As a result, the incorporated complexes acquire the water solubility while maintaining contact with the solution. Regarding the PB clathrate, the growth limitation enriched  $\text{Fe}^{\text{III}}$  ions with vacant coordination sites in the PB moiety, providing properties different from colloidal PB. The solubility to aqueous media, high stability under alkaline conditions, and electrochemical activity of the interior PB allow the extensive application of PB@L134P as a novel type of PB material. The readily available clathrate with HL L134P may extend the applications of the three-dimensional complexes insoluble in aqueous media.

## EXPERIMENTAL SECTION

**Materials.** All manipulations were performed at ambient temperature and atmosphere unless indicated otherwise. Chemicals were purchased from Sigma-Aldrich Japan LLC (Tokyo, Japan) and Nacalai Tesque Inc. (Kyoto, Japan) and were used without further purification.

**Spectroscopy.** IR spectra were recorded on an FT/IR-4000 (Jasco Co., Tokyo, Japan) equipped with an ATR unit. The buffer solution of protein samples was replaced with distilled water using a desalting column prior to the measurement. A droplet of the protein solution placed on the ATR unit was dried by blowing it with air at ambient temperature.

UV-Vis spectra were recorded on a U-3500 spectrophotometer (Hitachi High-Tech. Co., Tokyo, Japan). The sample concentration was adjusted to 0.3  $\mu\text{M}$  protein based on the result of the Bradford protein assay or 20  $\mu\text{M}$   $\text{Fe}_4[\text{Fe}(\text{CN})_6]_3$  based on the molar extinction coefficients calculated from that for PB nanoparticles ( $2.4 \times 10^4 \text{ M}^{-1}\text{cm}^{-1}$  at 700 nm, See SI).

The far-UV CD spectrum (200-250 nm) was recorded on a J-720 spectropolarimeter (Jasco Co., Tokyo, Japan) equipped with a Peltier-type cell temperature controller. The sample concentration was adjusted to 0.3  $\mu$ M protein based on the Bradford protein assay.

**Transmission electron microscopy (TEM).** TEM images were recorded on a JEM-1010 transmission electron microscope (JEOL Co., Tokyo, Japan) equipped with a FastScan-F214 (T) Charge-Coupled Device (CCD) camera (TVIPS, Gauting, Germany) at 80 kV. Protein samples (24 mg/L in HEPES buffer) were stained with 2% ammonium molybdate tetrahydrate (w/v) for 1 min and air-dried.

**MALDI-TOF mass spectrometry.** MALDI-TOF mass spectra were recorded on Bruker autoflex speed TOF/TOF (Bruker Japan Co., Yokohama, Japan). Following agents were used as calibrants: Angiotensin2 (Monoisotopic mass = 1047.189); Substance\_P (1348.642); ACTH fragment(2094.427); Somatostatin (3149.574); Insulin (5734.520). The mass accuracy was estimated to be 100ppm. A sample solution treated with proteinase K was desalted using a desalting column (PD-10, GE Healthcare Japan Co., Tokyo, Japan) preequilibrated with distilled water. The desalted solution was concentrated to 100  $\mu$ L and mixed with  $\alpha$ -Cyano-4-hydroxycinnamic acid as the matrix.

**Electrochemical measurement.** Electrochemical measurements were performed with an ALS-600C (BAS Co., Tokyo, Japan) electrochemical instrument. A standard three-electrode cell was used, where a glassy carbon electrode (3 mm diameter), Pt wire, and Ag/AgCl electrode served as the working electrode, counter electrode, and reference electrode, respectively. The concentration of PB@L134P was adjusted to 80  $\mu$ M based on the absorbance at 700 nm and the extinction coefficient of  $\text{Fe}_4[\text{Fe}(\text{CN})_6]_3$  ( $2.5 \times 10^4 \text{ M}^{-1}\text{cm}^{-1}$ ) in a 0.1 M KCl solution. All potentials were measured with respect to the standard hydrogen electrode (SHE).

**Gel permeation Chromatography.** Gel permeation chromatography was performed on Sephacryl S-300 HR (Cytiva Tokyo, Japan) preequilibrated with HEPES buffer containing 0.1 M sodium chloride. The flow rate of the elution buffer was set to 0.5 mL min<sup>-1</sup>. The protein elution was monitored by UV absorption at 280 nm.

**Quantification of Cu ion.** Copper ions were quantified using ICP-AES (ICPE-9820, Shimadzu Co., Kyoto, Japan). A protein sample in HEPES buffer was desalted using a PD-10 desalting column preequilibrated with distilled water. The desalted solution (1mL) was mixed with 60% HNO<sub>3</sub> solution (2 mL) in the glass vessel that was pre-treated with 60% HNO<sub>3</sub>. The mixture was heated until immediately before drying, and the resulting solution was diluted to 5 mL with 0.1 M HNO<sub>3</sub> for measurement.

**Preparation of the HL L134P mutant.** An expression vector for horse L-chain ferritin pET-FrWT, in which the gene was inserted at the *Nde*I and *Bam*HI restriction enzyme sites of pET-11a, was a kind gift from Takahumi Ueno, Tokyo Institute of Technology. An expression vector for HL L134P was constructed using the Quick Change® Site-Directed Mutagenesis Kit (Stratagene Co., Santa Clara, CA) and pET-FrWT as the template. The following sequence and complementary strand were used as primers to insert the mutation: 5'-GGAGAGCCACTTCCCGGACGAGGAGGTGAAAC-3'. The underlined sequences correspond to the Pro mutant. The resulting plasmid was transferred into a bacterial strain, *E. coli* BL21(DE3). The transformed strain was aerobically cultured in the LB medium at 37°C. After initial growth, the bacterial culture was added isopropyl  $\beta$ -D-1-thiogalactopyranoside to 1 mM to initiate overproducing the mutant protein, followed by further culturing for 7 hrs.

The recombinant HL L134P was purified using the same method as the wild type protein.<sup>51</sup> The protein purity was monitored after each step using SDS-PAGE, which confirmed that greater than

95% purity was achieved after all purification procedures (Figure S2a). The concentration of the purified protein was determined with the Bradford method and Quick Start™ Bradford (Bio-Rad Lab. Inc., Hercules, CA) for protein staining. The molar extinction coefficient at 278 nm was calculated to be  $4.6 \times 10^5 \text{ M}^{-1}\text{cm}^{-1}$ . The purified protein was stored in 20 mM HEPES-NaOH (HEPES) buffer at pH 7.0 until use in the synthesis of PB@L134P.

**Synthesis of PB@L134P.** After changing the buffer to 1 M sodium acetate (NaOAc) at pH 4.2, using PD-10 desalting column, HL L134P (2  $\mu\text{M}$ ) was mixed with 2 mM copper acetate and incubated overnight. Unreacted copper ion was removed with the desalting column preequilibrated with NaOAc buffer, and the eluate was subsequently dialyzed against the same buffer. After adjusting the concentration to 2  $\mu\text{M}$ , the resulting protein was reacted with 2 mM  $\text{K}_3[\text{Fe}(\text{CN})_6]$  in 20 mM NaOAc buffer at pH 4.2 to gradually form a yellow precipitate, which was collected by centrifugation and rinsed with HEPES buffer. Subsequent exposure to 100 mM iron(II) sulfate under an  $\text{N}_2$  atmosphere in HEPES buffer changed the color of the recovered precipitate from yellow to blue within 24 hrs. The resulting bluish precipitate was repeatedly washed with HEPES buffer until the effluent became unresponsive to the colorimetric detection of  $\text{Fe}^{\text{II}}$  ions using phenanthroline. Extensive sonication in HEPES buffer helped solubilize the blueish solid. The obtained blue solution was further purified with the desalting column and dialyzed against HEPES buffer.

**Evaluation of stability in alkaline solutions.** The stability of PB@L134P, colloidal PB, and PB@L134P digested with protease K in alkaline solutions was evaluated by monitoring the disappearance of the IVCT band in the absorption spectrum. The solution pH ranged from 8 to 10 and was prepared by adding 2 M NaOH to HEPES buffer or 20 mM CHES-NaOH at pH 9.0 (CHES) buffer. The kinetic plots for each sample were obtained from the average of 3 independent

experiments. The obtained decay curves of the IVCT bands were tentatively analyzed with the first-order kinetics.

**Protein digestion of PB@L134P with Proteinase K.** A mixture of 1  $\mu\text{M}$  PB@L134P and 3 units of proteinase K in HEPES buffer was allowed to stand for 24 hrs at ambient temperature. Completion of the protein digestion was confirmed by SDS-PAGE (Figure 5). Removal of the digested protein from the PB moiety was performed on a gel permeation column preequilibrated with HEPES buffer. A blue-colored fraction was collected and concentrated by ultrafiltration for further experiments.

**Reaction with potassium cyanide.** A 100 mM KCN solution of HEPES buffer was added to PB@L134P in HEPES buffer (20  $\mu\text{M}$  based on  $\text{Fe}_4[\text{Fe}(\text{CN})_6]_3$ ) to a final concentration of 1 mM. The reaction mixture was allowed to stand for 30 min and subsequently subjected to the desalting column operation to remove unreacted KCN. Due to the lack of extinction coefficient data for KCN treated  $\text{Fe}_4[\text{Fe}(\text{CN})_6]_3$ , the protein concentration of the KCN treated PB@L134P determined by the Bradford method was used to prepare the sample solution in further experiments.

**Measurement of the catalytic activity.** The catalytic activity of PB@L134P was studied under aerobic conditions. The concentration of PB@L134P was adjusted to 1.0  $\mu\text{M}$ , based on  $\text{Fe}_4[\text{Fe}(\text{CN})_6]_3$  in 200 mM NaOAc buffer at pH 3.6 with 160  $\mu\text{M}$  TMB and 100  $\mu\text{M}$   $\text{H}_2\text{O}_2$ . The oxidation products of TMB were traced by monitoring the increase in absorption bands at 653 nm ( $\epsilon = 3.9 \times 10^4 \text{ M}^{-1}\text{cm}^{-1}$ )<sup>56</sup> using the UV-Vis spectrometer. The concentration of colloidal PB and PB@L134P after the protease K digestion was adjusted so that the absorbance at 700 nm was identical to PB@L134P used for the catalytic reaction. The concentration of PB@L134P after the KCN treatment was adjusted so that the protein concentration was identical to PB@L134P used

for the catalytic reaction. The kinetic plots for each catalyst were obtained from the average of 3 independent experiments.

**Iodometric titration of  $\text{H}_2\text{O}_2$ .**<sup>57</sup> The following experiments were performed at least three times to determine the concentrations of sodium thiosulfate ( $\text{Na}_2\text{S}_2\text{O}_3$ ) and  $\text{H}_2\text{O}_2$ . A solution of  $\text{Na}_2\text{S}_2\text{O}_3$  was standardized by titrating with a mixture of 1.0 mL of  $\text{KIO}_3$  (100  $\mu\text{M}$ ) in 200 mM NaOAc buffer at pH 3.6 and 5.0 mL of 10% KI solution (0.1 g  $\text{mL}^{-1}$ ) including 1.0 mL of 1 M HCl. After the  $\text{KIO}_3$  solution became light yellow, a starch solution was added. The titration continued until the blue color disappeared. A mixture of  $\text{H}_2\text{O}_2$  (100  $\mu\text{M}$ ) and PB@L134P (1.0  $\mu\text{M}$  based on  $\text{Fe}_4[\text{Fe}(\text{CN})_6]_3$ ) in the 200 mM NaOAc buffer was allowed to stand and sampled every 30 min for the reaction with the standardized  $\text{Na}_2\text{S}_2\text{O}_3$  solution. The residual  $\text{Na}_2\text{S}_2\text{O}_3$  was determined by the titration mentioned above to evaluate the concentration of  $\text{H}_2\text{O}_2$  consumed in the mixture with PB@L134P.

## ASSOCIATED CONTENT

### Supporting Information

The following Supporting Information is available free of charge on the ACS Publications website: UV-Vis spectra, CD spectra, cyclic voltammograms, TEM images, an SDS-PAGE gel image, a photo of PB@L134P dissolved in HEPES buffer, plots showing catalytic activities of PB@L134P in different forms, protein alignments, and protein fragments listed in Table 1.

## AUTHOR INFORMATION

### Corresponding Author

\*Hiroshi Nakajima, e-mail: [hnakajima@osaka-cu.ac.jp](mailto:hnakajima@osaka-cu.ac.jp)

### ORCID

Hiroshi Nakajima: 0000-0002-0079-1274

Takanori Nishioka: 0000-0002-4968-8059

Shigetoshi Aono: 0000-0002-2870-3694

Makoto Miyata: 0000-0002-7478-7390

Yuhei O Tahara: 0000-0002-2736-9233

### Notes

The authors declare no competing financial interests.

## ACKNOWLEDGMENTS



This study was supported by the Cooperative Study Program of Exploratory Research Center on Life and Living Systems (ExCELLS program No.19-317), JSPS KAKENHI Grant Numbers JP17J11464 and JP16K05729, a Grant-in-Aid for Strategic Research of Osaka City University, and a Grant-in-Aid 2019 from the Koyanagi Research Foundation.

#### ABBREVIATIONS

PB, Prussian blue; TEM, transmission electron microscope; TMB, 3,3',5,5'-tetramethylbenzidine; HEPES, 4-(2-hydroxyethyl)-1-piperazineethanesulfonic acid; CHES, 2-(cyclohexyl amino) ethanesulfonic acid; CD, circular dichroism

## REFERENCES

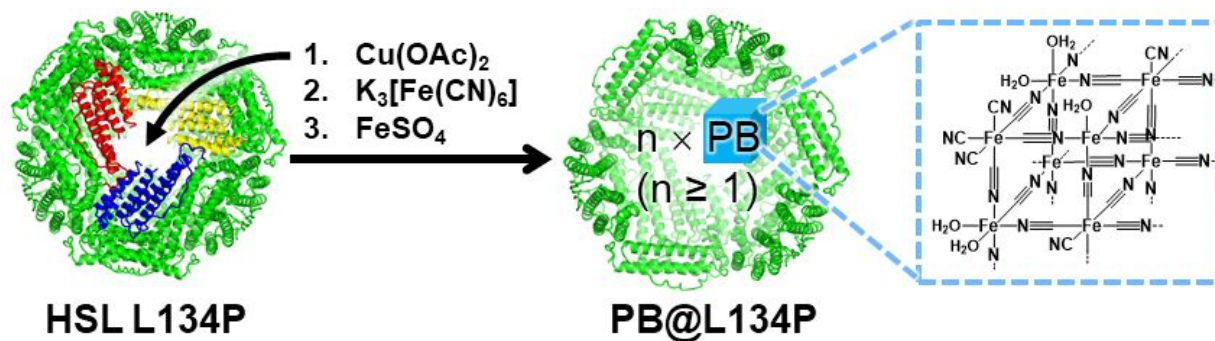
- (1) Harrison, P. M.; Arosio, P. Ferritins: Molecular properties, iron storage function and cellular regulation *Biochim. Biophys. Acta-Bioenerg.* **1996**, 1275 (3), 161-203.
- (2) Liu, X. F.; Theil, E. C. Ferritins: Dynamic management of biological iron and oxygen chemistry *Accounts Chem. Res.* **2005**, 38 (3), 167-175.
- (3) Proulxcurry, P. M.; Chasteen, N. D. Molecular aspects of iron uptake and storage in ferritin *Coord. Chem. Rev.* **1995**, 144, 347-368.
- (4) Behera, R. K.; Torres, R.; Tosha, T.; Bradley, J. M.; Goulding, C. W.; Theil, E. C. Fe<sup>2+</sup> substrate transport through ferritin protein cage ion channels influences enzyme activity and biomineralization *J. Biol. Inorg. Chem.* **2015**, 20 (6), 957-969.
- (5) Bernacchioni, C.; Ghini, V.; Theil, E. C.; Turano, P. Modulating the permeability of ferritin channels *RSC Adv.* **2016**, 6 (25), 21219-21227.
- (6) Takagi, H.; Shi, D. S.; Ha, Y.; Allewell, N. M.; Theil, E. C. Localized unfolding at the junction of three ferritin subunits - A mechanism for iron release? *J. Biol. Chem.* **1998**, 273 (30), 18685-18688.
- (7) Liu, X. F.; Jin, W. L.; Theil, E. C. Opening protein pores with chaotropes enhances Fe reduction and chelation of Fe from the ferritin biomineral *Proc. Natl. Acad. Sci. U. S. A.* **2003**, 100 (7), 3653-3658.
- (8) Tosha, T.; Behera, R. K.; Theil, E. C. Ferritin Ion channel disorder inhibits Fe(II)/O<sub>2</sub> reactivity at distant sites *Inorg. Chem.* **2012**, 51 (21), 11406-11411.
- (9) Hasan, M. R.; Tosha, T.; Theil, E. C. Ferritin contains less Iron (Fe<sup>59</sup>) in cells when the protein pores are unfolded by mutation *J. Biol. Chem.* **2008**, 283 (46), 31394-31400.
- (10) Sala, D.; Ciambellotti, S.; Giachetti, A.; Turano, P.; Rosato, A. Investigation of the iron(II) release mechanism of human H-ferritin as a function of pH *J. Chem. Inf. Model* **2017**, 57 (9), 2112-2118.
- (11) Jutz, G.; van Rijn, P.; Miranda, B. S.; Boker, A. Ferritin: A versatile building block for bionanotechnology *Chem. Rev.* **2015**, 115 (4), 1653-1701.
- (12) Truffi, M.; Fiandra, L.; Sorrentino, L.; Monieri, M.; Corsi, F.; Mazzucchelli, S. Ferritin nanocages: A biological platform for drug delivery, imaging and theranostics in cancer *Pharmacol. Res.* **2016**, 107, 57-65.
- (13) Takezawa, Y.; Bockmann, P.; Sugi, N.; Wang, Z. Y.; Abe, S.; Murakami, T.; Hikage, T.; Erker, G.; Watanabe, Y.; Kitagawa, S.; Ueno, T. Incorporation of organometallic Ru complexes into apo-ferritin cage *Dalton Trans.* **2011**, 40 (10), 2190-2195.
- (14) Webb, B.; Frame, J.; Zhao, Z.; Lee, M. L.; Watt, G. D. Molecular entrapment of small molecules within the interior of horse spleen ferritin *Arch. Biochem. Biophys.* **1994**, 309 (1), 178-183.
- (15) Yang, Z.; Wang, X. Y.; Diao, H. J.; Zhang, J. F.; Li, H. Y.; Sun, H. Z.; Guo, Z. J. Encapsulation of platinum anticancer drugs by apoferritin *Chem. Commun.* **2007**, (33), 3453-3455.
- (16) Mazzucchelli, S.; Truffi, M.; Baccarini, F.; Beretta, M.; Sorrentino, L.; Bellini, M.; Rizzuto, M. A.; Ottria, R.; Ravelli, A.; Ciuffreda, P.; Prosperi, D.; Corsi, F. H-Ferritin-nanocaged olaparib: a promising choice for both BRCA-mutated and sporadic triple negative breast cancer *Sci Rep* **2017**, 7,
- (17) Liu, M. M.; Zhu, Y.; Wu, T. T.; Cheng, J. J.; Liu, Y. Z. Nanobody-ferritin conjugate for targeted photodynamic therapy *Chem.-Eur. J.* **2020**, 26 (33), 7442-7450.

- (18) Galvez, N.; Sanchez, P.; Dominguez-Vera, J. M. Preparation of Cu and CuFe Prussian blue derivative nanoparticles using the apoferritin cavity as nanoreactor *Dalton Trans.* **2005**, (15), 2492-2494.
- (19) Ferraro, G.; Ciambellotti, S.; Messori, L.; Merlino, A. Cisplatin binding sites in human H-chain ferritin *Inorg. Chem.* **2017**, 56 (15), 9064-9070.
- (20) Ciambellotti, S.; Pratesi, A.; Severi, M.; Ferraro, G.; Alessio, E.; Merlino, A.; Messori, L. The NAMI A - human ferritin system: a biophysical characterization *Dalton Trans.* **2018**, 47 (33), 11429-11437.
- (21) Ahn, B.; Lee, S. G.; Yoon, H. R.; Lee, J. M.; Oh, H. J.; Kim, H. M.; Jung, Y. Four-fold channel-nicked human ferritin nanocages for active drug loading and pH-responsive drug release *Angew. Chem.-Int. Edit.* **2018**, 57 (11), 2909-2913.
- (22) Hempstead, P. D.; Yewdall, S. J.; Fernie, A. R.; Lawson, D. M.; Artymiuk, P. J.; Rice, D. W.; Ford, G. C.; Harrison, P. M. Comparison of the three-dimensional structures of recombinant human H and horse L ferritins at high resolution *J. Mol. Biol.* **1997**, 268 (2), 424-448.
- (23) Liu, X. F.; Theil, E. C. Ferritin reactions: Direct identification of the site for the diferriic peroxide reaction intermediate *Proc. Natl. Acad. Sci. U. S. A.* **2004**, 101 (23), 8557-8562.
- (24) Chasteen, N. D.; Harrison, P. M. Mineralization in ferritin: An efficient means of iron storage *J. Struct. Biol.* **1999**, 126 (3), 182-194.
- (25) Pozzi, C.; Ciambellotti, S.; Bernacchioni, C.; Di Pisa, F.; Mangani, S.; Turano, P. Chemistry at the protein-mineral interface in L-ferritin assists the assembly of a functional ( $\mu^3$ -oxo)Tris ( $\mu^2$ -peroxo) triiron(III) cluster *Proc. Natl. Acad. Sci. U. S. A.* **2017**, 114 (10), 2580-2585.
- (26) Ware, M. Prussian blue: Artists' pigment and chemists' sponge *J. Chem. Educ.* **2008**, 85 (5), 612-620.
- (27) Herren, F.; Fischer, P.; Ludi, A.; Halg, W. Neutron-diffraction study of Prussian blue,  $\text{Fe}_4\text{Fe}(\text{CN})_6 \cdot 3\text{H}_2\text{O}$  - Location of water-molecules and long-range magnetic order *Inorg. Chem.* **1980**, 19 (4), 956-959.
- (28) Neff, V. D. Electrochemical oxidation and reduction of thin-films of Prussian blue *J. Electrochem. Soc.* **1978**, 125 (6), 886-887.
- (29) Lee, K. M.; Tanaka, H.; Takahashi, A.; Kim, K. H.; Kawamura, M.; Abe, Y.; Kawamoto, T. Accelerated coloration of electrochromic device with the counter electrode of nanoparticulate Prussian blue-type complexes *Electrochim. Acta* **2015**, 163, 288-295.
- (30) Borzenkov, M.; D'Alfonso, L.; Polissi, A.; Sperandio, P.; Collini, M.; Dacarro, G.; Taglietti, A.; Chirico, G.; Pallavicini, P. Novel photo-thermally active polyvinyl alcohol-Prussian blue nanoparticles hydrogel films capable of eradicating bacteria and mitigating biofilms *Nanotechnology* **2019**, 30 (29), 295702.
- (31) Li, W. P.; Su, C. H.; Tsao, L. C.; Chang, C. T.; Hsu, Y. P.; Yeh, C. S. Controllable CO release following near infrared light-induced cleavage of iron carbonyl derivatized Prussian blue nanoparticles for CO-assisted synergistic treatment *ACS Nano* **2016**, 10 (12), 11027-11036.
- (32) Fu, G. L.; Liu, W.; Feng, S. S.; Yue, X. L. Prussian blue nanoparticles operate as a new generation of photothermal ablation agents for cancer therapy *Chem. Commun.* **2012**, 48 (94), 11567-11569.
- (33) Bleuzen, A.; Lomenech, C.; Escax, V.; Villain, F.; Varret, F.; Moulin, C. C. D.; Verdaguer, M. Photoinduced ferrimagnetic systems in Prussian blue analogues  $\text{C}^{\text{I}}_x\text{Co}_4[\text{Fe}(\text{CN})_6]_y$  ( $\text{C}^{\text{I}}$  = alkali cation). 1. Conditions to observe the phenomenon *J. Am. Chem. Soc.* **2000**, 122 (28), 6648-6652.
- (34) Ohkoshi, S.; Tokoro, H.; Hashimoto, K. Temperature- and photo-induced phase transition in rubidium manganese hexacyanoferrate *Coord. Chem. Rev.* **2005**, 249 (17-18), 1830-1840.

- (35) Itaya, K.; Shoji, N.; Uchida, I. Catalysis of the reduction of molecular-oxygen to water at Prussian blue modified electrodes *J. Am. Chem. Soc.* **1984**, 106 (12), 3423-3429.
- (36) Tabe, H.; Terashima, C.; Yamada, Y. Effect of surface acidity of cyano-bridged polynuclear metal complexes on the catalytic activity for the hydrolysis of organophosphates *Catal. Sci. Technol.* **2018**, 8 (18), 4747-4756.
- (37) Zhang, W.; Hu, S. L.; Yin, J. J.; He, W. W.; Lu, W.; Ma, M.; Gu, N.; Zhang, Y. Prussian blue nanoparticles as multienzyme mimetics and reactive oxygen species scavengers *J. Am. Chem. Soc.* **2016**, 138 (18), 5860-5865.
- (38) Dominguez-Vera, J. M.; Colacio, E. Nanoparticles of Prussian blue ferritin: A new route for obtaining nanomaterials *Inorg. Chem.* **2003**, 42 (22), 6983-6985.
- (39) Okuda, M.; Eloi, J. C.; Jones, S. E. W.; Sarua, A.; Richardson, R. M.; Schwarzacher, W. Fe<sub>3</sub>O<sub>4</sub> nanoparticles: protein-mediated crystalline magnetic superstructures *Nanotechnology* **2012**, 23 (41), 415601.
- (40) Chandramouli, B.; Bernacchioni, C.; Di Maio, D.; Turano, P.; Brancato, G. Electrostatic and structural bases of Fe<sup>2+</sup> translocation through ferritin channels *J. Biol. Chem.* **2016**, 291 (49), 25617-25628.
- (41) Crichton, R. R.; Declercq, J. P. X-ray structures of ferritins and related proteins *Biochim. Biophys. Acta-Gen. Subj.* **2010**, 1800 (8), 706-718.
- (42) Watt, R. K.; Hilton, R. J.; Graff, D. M. Oxido-reduction is not the only mechanism allowing ions to traverse the ferritin protein shell *Biochim. Biophys. Acta-Gen. Subj.* **2010**, 1800 (8), 745-759.
- (43) Marquez, C.; Cirujano, F. G.; Smolders, S.; Van Goethem, C.; Vankelecom, I.; De Vos, D.; De Baerdemaeker, T. Metal ion exchange in Prussian blue analogues: Cu(II)-exchanged Zn-Co PBAs as highly selective catalysts for A(3) coupling *Dalton Trans.* **2019**, 48 (12), 3946-3954.
- (44) Mazur, A.; Litt, I.; Shorr, E. Chemical properties of ferritin and their relation to its vasodepressor activity *J. Biol. Chem.* **1950**, 187 (2), 473-484.
- (45) Ueno, T.; Abe, M.; Hirata, K.; Abe, S.; Suzuki, M.; Shimizu, N.; Yamamoto, M.; Takata, M.; Watanabe, Y. Process of accumulation of metal ions on the interior surface of apo-ferritin: crystal structures of a series of apo-ferritins containing variable quantities of Pd(II) ions *J. Am. Chem. Soc.* **2009**, 131 (14), 5094-5100.
- (46) Tosha, T.; Ng, H. L.; Bhattasali, O.; Alber, T.; Theil, E. C. Moving metal ions through ferritin-protein nanocages from three-fold pores to catalytic sites *J. Am. Chem. Soc.* **2010**, 132 (41), 14562-14569.
- (47) Valentini, M. T. G.; Stella, R.; Cola, M. Characterization of copper hexacyanoferrate(II) and (III) with reference to their use as cesium adsorbers *J. Radioanal. Nucl. Chem.-Artic.* **1986**, 102 (1), 99-110.
- (48) Ciambellotti, S.; Pozzi, C.; Mangani, S.; Turano, P. Iron biomineral growth from the initial nucleation seed in L-ferritin *Chem.-Eur. J.* **2020**, 26 (26), 5770-5773.
- (49) Karyakin, A. A. Prussian blue and its analogues: Electrochemistry and analytical applications *Electroanalysis* **2001**, 13 (10), 813-819.
- (50) Kim, M.; Rho, Y.; Jin, K. S.; Ahn, B.; Jung, S.; Kim, H.; Ree, M. pH-dependent structures of ferritin and apoferritin in solution: disassembly and reassembly *Biomacromolecules* **2011**, 12 (5), 1629-1640.
- (51) Niemeyer, J.; Abe, S.; Hikage, T.; Ueno, T.; Erker, G.; Watanabe, Y. Noncovalent insertion of ferrocenes into the protein shell of apo-ferritin *Chem. Commun.* **2008**, (48), 6519-6521.

- (52) Xu, D. G.; Watt, G. D.; Harb, J. N.; Davis, R. C. Electrical conductivity of ferritin proteins by conductive AFM *Nano Lett.* **2005**, 5 (4), 571-577.
- (53) Axford, D. N.; Davis, J. J. Electron flux through apo- and holoferritin *Nanotechnology* **2007**, 18 (14), 145502.
- (54) Zhang, W.; Zhang, Y.; Chen, Y. H.; Li, S. Y.; Gu, N.; Hu, S. L.; Sun, Y.; Chen, X.; Li, Q. Prussian blue modified ferritin as peroxidase mimetics and its applications in biological detection *J. Nanosci. Nanotechnol.* **2013**, 13 (1), 60-67.
- (55) Volpe, G.; Compagnone, D.; Draisci, R.; Palleschi, G. 3,3',5,5'-tetramethylbenzidine as electrochemical substrate for horseradish peroxidase based enzyme immunoassays. A comparative study *Analyst* **1998**, 123 (6), 1303-1307.
- (56) Marquez, L. A.; Dunford, H. B. Mechanism of the oxidation of 3,5,3',5'-tetramethylbenzidine by myeloperoxidase determined by transient- and steady-state kinetics *Biochemistry* **1997**, 36 (31), 9349-9355.
- (57) Xiong, Y.; Wang, Q.; Li, X.; Fang, S. W.; Duan, M. Total sulfur dioxide determination in red wine by suppressed ion chromatography with in-sample oxidation and SPE *Chromatographia* **2018**, 81 (7), 1003-1011.

## For Table of Contents Only



A new method to produce Prussian blue (PB) clathrate with ferritin without the need to disassemble and reassemble the protein was developed using the horse spleen L-ferritin L134P mutant (HSL L134P), in which  $C_3$  axis channels were anticipated to be in an open conformation. The prepared clathrate (PB@L134P) was soluble in water and reproduced the spectroscopic and electrochemical properties of colloidal PB prepared using the conventional method. The significantly improved stability of PB@L134P in alkaline solutions suggests that the clathrate may have potential applications as an alternative to conventional PB.